Asia Pacific Research Initiative for Sustainable Energy Systems 2011 (APRISES11)

Office of Naval Research
Grant Award Number N0014-12-1-0496

Methane Hydrates:

Effect of the Properties of Porous Media on Hydrate Stability

Task 3.1

May 2014

HNEI
Hawai'i Natural Energy Institute
University of Hawai'i at Mānoa

MS Plan B report

Effect of the Properties of Porous Media on Hydrate Stability

Master of Science in Ocean & Resources Engineering

May 2014

By Shino Miyakita

Committee: Stephen M. Masutani, Chair
Gerard C. Nihous
John C. Wiltshire

ABSTRACT

Calorimetric experiments were performed to test the hypothesis that the pressure-temperature phase boundaries of methane hydrate change when formation and dissociation occur in porous media. Two "standard" sands selected by the national methane hydrate R&D programs in Japan and the U.S. were employed in these experiments. The data suggest that a small shift in the phase boundary of hydrates might occur in porous media. The measured change is of the order of scatter in the experimental data but is consistent. For both sands, and over a range of pressures relevant to deep ocean sediments, the phase boundary for a simple water-methane binary system tends to overpredict hydrate melting temperature. Lower melting temperatures imply that natural hydrate deposits in seafloor sediment are more vulnerable to purposeful or inadvertent increases in temperature. While this can be advantageous for certain methane recovery strategies, it raises concerns about outgassing and seafloor stability in a warming climate. Additional experiments appear to be warranted to confirm this phenomenon for a broader range of porous media properties and to more definitively quantify the shift in the phase boundary and to understand the underlying mechanism.

TABLE OF CONTENTS

LIST OF TABLES

LIST OF FIGURES

NOMENCLATURE

Apparent Density (g/cm^3): density of sand grain material excluding pores reported in Table 4.1.2

Bulk Density (g/cm^3): density of sand grain material including pores reported in Table 4.1.2

Gs: specific gravity (g/m^3) of sand particles determined by ASTM D854

n: intergranular percent porosity of sand (%) used in Table 4.2.1; n ≡ void space between sand grains/total volume of sample x 100

Specific Surface Area (cm^2/g): total surface area reported in Table 4.1.3 including pores per unit mass of sand material determined by gas adsorption

Sr: Specific water saturation (%) of the sample used in Table 4.2.1; percentage of the volume of the sample in the calorimeter that is water

Total Intrusion Volume (cm^3/g): measured volume of mercury that is forced into pores of the sand grain surface per unit mass of sand grain material; reported in Table 4.1.2

Total Pore Area (m^2/g): calculated total volume of surface pores per unit mass of sand grain material; reported in Table 4.2.1

Volume Median Pore Diameter (μm): calculated using Washburn's equation using mercury porosimetry data; pore diameter where 50% of the total volume of mercury has been added

ω_n: Natural water content (%) of sand particles determined by ASTM D2216; this value depends on ambient conditions

1. INTRODUCTION

Hydrates are solids consisting of a crystal lattice of water enclosing various guest molecules (Sloan *et al*., 2007). Hydrates in seafloor sediment and Arctic permafrost represent a huge natural reservoir of methane (Boswell & Collett, 2011). Industrial production of methane fuel from this resource requires the development of economical and environmentally acceptable methods. It is generally believed that hydrates should be dissociated *in situ* and the released methane gas collected and removed using methods such as pressure reduction, thermal stimulation, inhibitor injection, geothermal stimulation, or *in situ* combustion (Trofimuk, 1982). Since methane is a hydrocarbon fossil fuel, oxidation for energy applications will release CO_2. In order to reduce carbon emissions into the atmosphere, it has been proposed that methane hydrate be replaced with CO_2 hydrate during the recovery process as a sequestration strategy, since CH_4 and CO_2 hydrates have similar pressure-temperature stability properties (Nago& Nieto, 2011). Replacement would also reduce seafloor or permafrost subsidence problems.

Understanding the mechanisms of hydrate formation and dissociation in porous media is critical in order to devise viable methane extraction and carbon sequestration methods and to assess the associated environmental consequences. For example, Uchida *et al*. (2004) investigated the effects of porosity on the decomposition of methane hydrate formed in sediments and concluded: 1) that dissociation is mainly affected by intergranular pore size; and 2) that the hydrate phase equilibrium curves in porous media may be slightly different from those found in the literature which corresponds to simple binary methane-water samples. Their study, and other similar previous investigations, did not measure associated energy flows (e.g., heat of fusion; specific heat), which are important parameters for well production and environmental models. To investigate the mechanisms and energetics of methane hydrate formation and

decomposition in porous media, an experimental study was conducted employing calorimetry and Raman spectroscopy. Two types of sands which are representative of deep ocean methane hydrate sediments, and which are employed as standards in the Japanese and U.S. national methane hydrates research programs, were tested. Sandy sediments represent the most viable scenario for methane extraction. Measured phase transition temperatures of hydrates in these sands were compared with the phase diagram for the simple binary methane-water system.

2. OBJECTIVES

The technical objective of this study is:

- Conduct experiments of methane hydrate formation and dissociation in sand matrices using a Raman calorimeter to determine if hydrate stability is affected by the presence of the sand.

The primary hypothesis tested was:

- *Pressure-temperature phase boundaries of methane hydrate change when formation and dissociation occur in porous media.*

3. METHODS AND MATERIALS

3.1. Experimental Facility

Hydrate was formed as a simple two-component water-methane system and also in porous media employing a novel experimental facility which couples calorimetry with Raman spectroscopy. High pressure sample cells of a Setaram BT2.15 differential scanning calorimeter (DSC) have been modified to provide access for a fiberoptic probe to perform Raman measurements of the sample in the cell as it undergoes a user-defined thermal process. The calorimeter allows samples (up to about 8 ml) to be cooled or heated, according to a user-

selected process, between -196°C and 200°C at pressures up to ~10 MPa. The calorimeter can detect heat transfer to or from the sample as low as 0.10 μW and can be used to determine thermodynamic properties such as specific heats, heats of reaction, heats of fusion, and phase boundaries. Figure3.1.1 is a cutaway drawing of the DSC that shows its primary components. A photograph and schematic drawing of the experimental facility are shown in Figures.3.1.2 and 3.1.3, respectively.

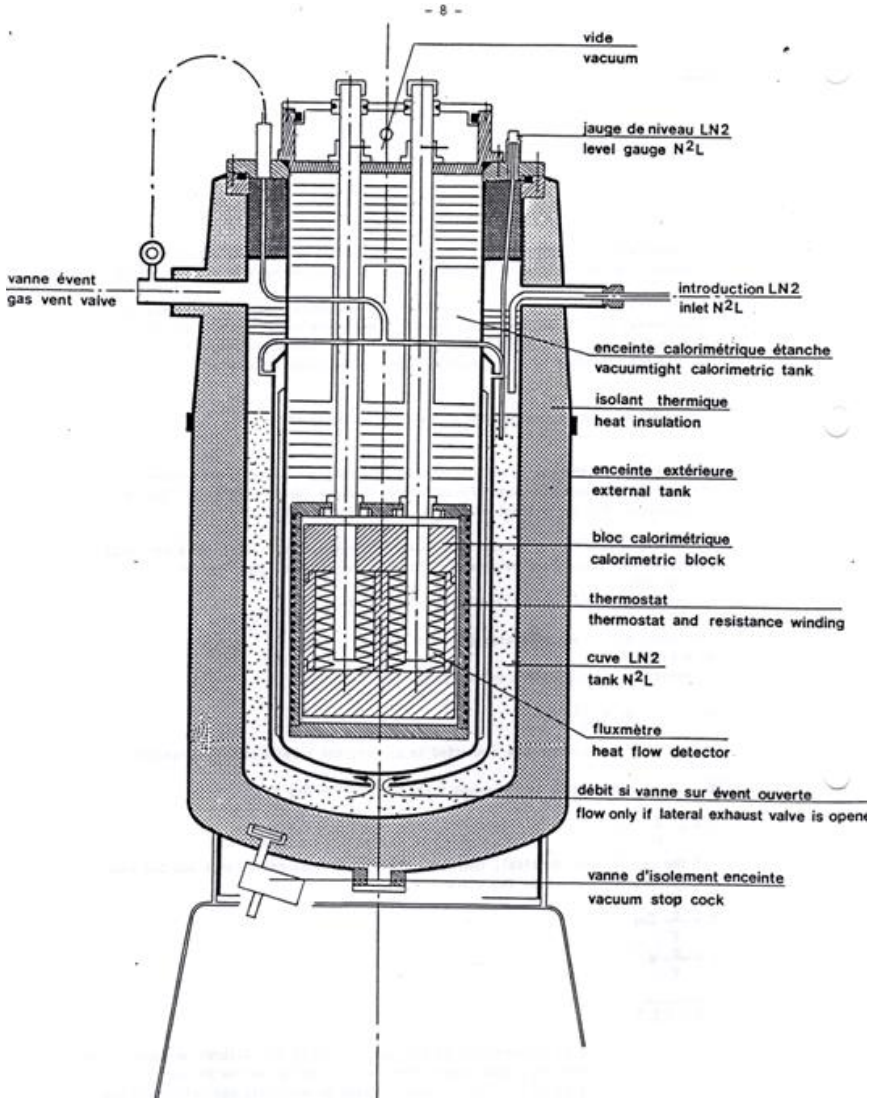

Figure 3.1.1 Cutaway drawing of the Setaram BT2.15 DSC

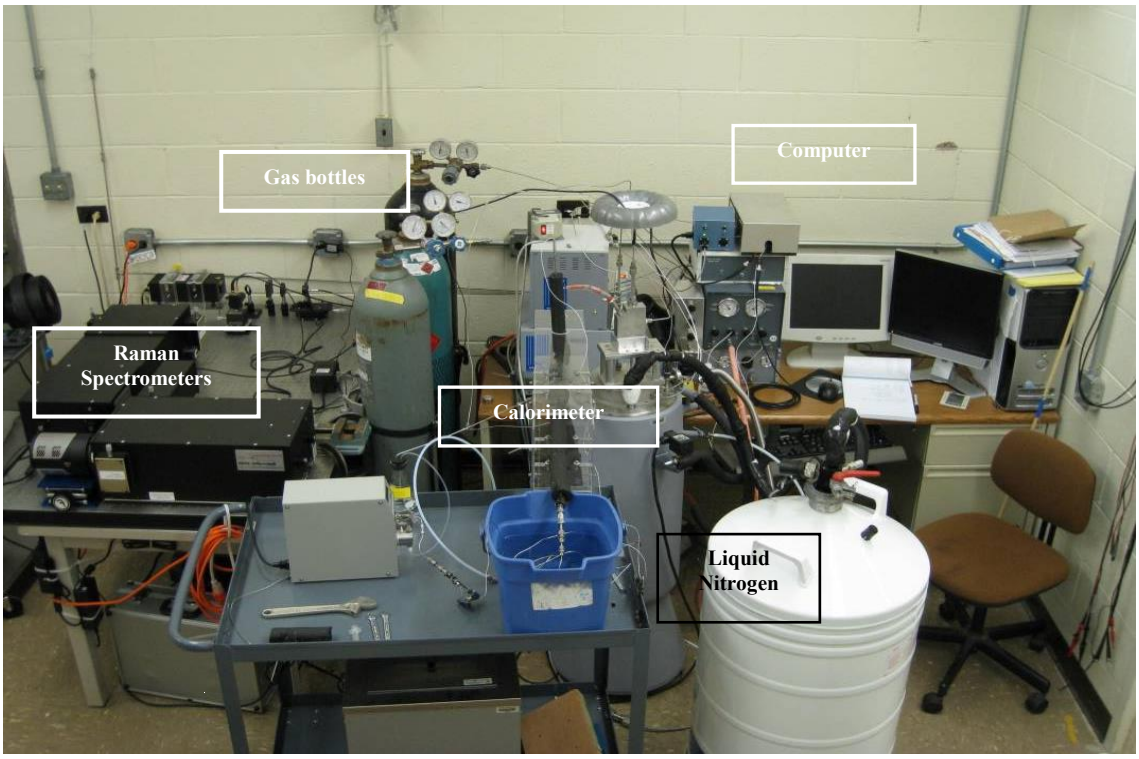

Figure 3.1.2 Photograph of the experimental facility

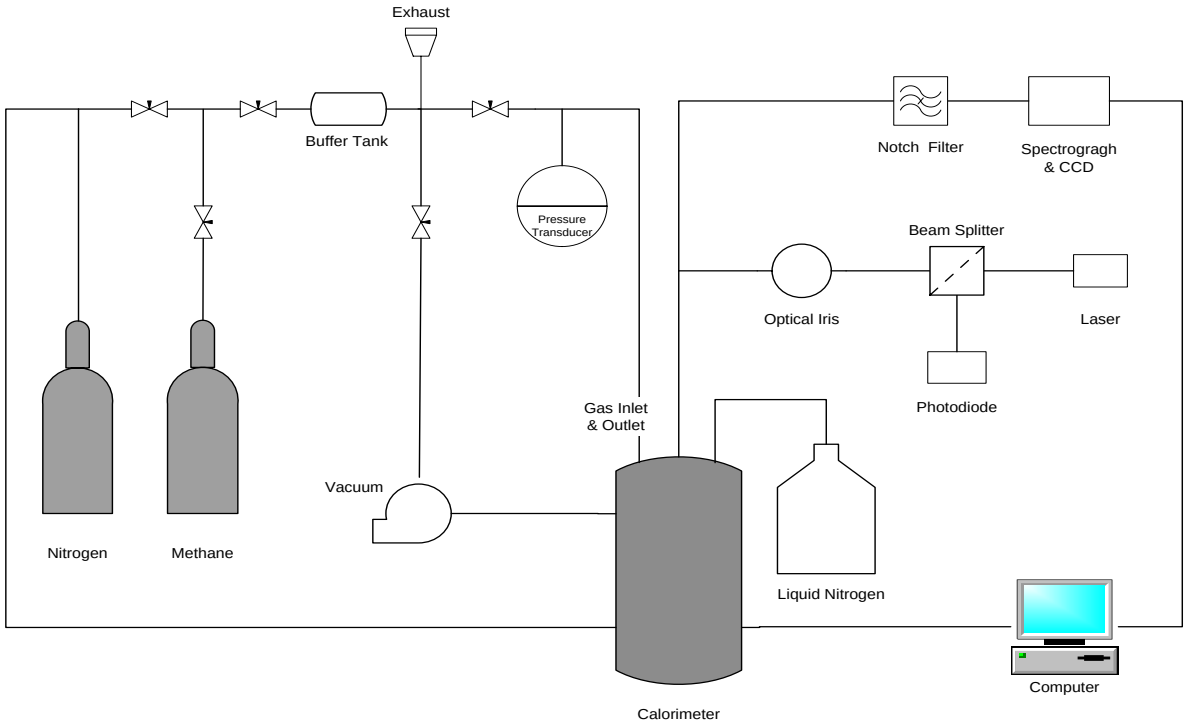

Figure 3.1.3 Schematic diagram of the experimental facility

The DSC monitors the difference in thermal energy required to change the temperature of a sample and a reference. The material being investigated is contained in closed cylindrical sample cell, which is inserted into a well in the DSC as shown in Figure 3.1.1. An identical empty sample cell is used as the reference and is inserted into a second adjacent well. The cells are completely surrounded by an array of thermocouples that detects the heat flow to or from each cell as temperature is changed with a combination of an electric furnace and a liquid N_2 cooling system.

Figure 3.1.4 shows a photograph of the fiberoptic probe assembly that extends into the pressurized sample cell through a compression fitting welded to its top closure. The 0.125 inch (3.175 mm) o.d. probe is inserted into a 0.250 inch (6.35 mm) o.d., 0.18 inch (4.57 mm) i.d., stainless steel tube that attaches to the compression fitting. This tube also provides access to the inside of the sample cell to add or remove gases. Raman spectroscopy is used to confirm the existence of methane hydrates in the sample during the experiment. The Raman system shown in Figures 3.1.2 and 3.1.3 comprises a solid state laser, the fiberoptic probe, and a spectrometer. Laser radiation at 532 nm is transmitted by a 200 μm core UV silica optical fiber into the cell to excite molecules in the sample to a virtual energy state. A portion of these excited molecules relax down to different rotation or vibrational levels than where they originally existed, with the emission of a photon. The frequency of the photon is shifted from the laser radiation. This Raman shift is determined by the structure of the molecule; i.e., its particular rotational and vibrational levels. Six 200 μm core optical fibers positioned around the transmitting fiber in the probe are used to collect the emitted Raman shifted light and bring it into a Princeton Instruments SpectraPro-2750 spectrograph equipped with a Princeton Instruments PIXIS ccd detector. The spectrograph has a focal length of 0.750 m.

Figure 3.1.4 Photograph of the fiberoptic probe assembly

The sample cell can be evacuated with a vacuum pump and purged with dry N_2 gas. Research grade methane gas is used to form hydrate in the sample cell during an experiment. A buffer tank filled with methane is connected to the gas supply line to minimize changes in sample pressure that occurs when hydrate forms or decomposes. With this system, pressure can generally be maintained to within ± 1%. An electronic pressure transducer is employed to continuously monitor and record sample pressure.

Two kinds of sand representative of deep ocean methane hydrate sediment were investigated: Toyoura sand, which has been adopted as the "standard" sand for the Japanese national methane hydrate R&D program (Hyodo *et al*., 2005) and Ottawa sand, which is the standard sand of the U.S. national program (Waite *et al.*, 2004). The properties of these sands, including composition, grain size distribution, void ratio and fraction, water saturation, and grain porosity, were determined to characterize the samples tested with the calorimeter. The general procedures that were employed are discussed below.

3.2. Procedures

3.2.1. Properties of porous media

Natural water content, specific gravity, and grain size distribution of the porous media employed in this investigation were determined following the respective standard procedures: ASTM D2216, ASTM D 854, and ASTM D 422. Scanning Electron Microscopy (SEM),

mercury intrusion porosimetry, and gas sorption analysis were used to characterize sand particle surfaces. The results of these tests for the sand samples are provided in Section 4.1.

3.2.2. Calorimeter experiments

Sand-water samples were prepared which have the desired porosity and specific water saturation for a particular experiment. The amount of sand needed to attain the target porosity was calculated based on the results of the specific gravity test. Next, distilled and deionized water was added to the sand. The amount of water was calculated considering the measured natural water content of the sand. The sand and water were mixed well and loaded into the calorimeter sample cell. The cell was closed and inserted into the calorimeter well before being purged with dry N_2 and vacuum evacuated. Methane gas was then added to the cell to achieve the desired pressure. The sample was then subjected to a user-selected thermal cycle to form and decompose hydrate and the thermal transfers indicative of phase transitions were monitored and recorded. Raman spectra were taken at selected points during the experiment to confirm the presence of methane hydrate.

4. RESULTS

4.1. Sand properties

The results of the natural water content test (ASTM D2216), the specific gravity test (ASTM D 854), and the grain size distribution test (ASTM D 422) for Toyoura and Ottawa sands are shown in Table 4.1.1. A portion of the Ottawa sand was sieved to remove fine particles and is identified as Ottawa* in the table. For comparison, the specific gravity of laboratory silica sand also is provided. The cumulative particle size distribution curves for the Toyoura, Ottawa, and Ottawa* sands are plotted in Figure 4.1.1.

	Natural water content (%): ω_n	Specific gravity (g/cm^3): G_s	Grain size distribution by weight (%)	
			140–425 (μm)	< 75 (μm)
Toyoura	0.3267	2.656	99.85	0.01
Ottawa	0.3010	2.671	81.81	3.54
Ottawa*	0.2277	2.672	84.81	0
Silica	–	≈ 2.700	–	–

Table 4.1.1 Sand properties

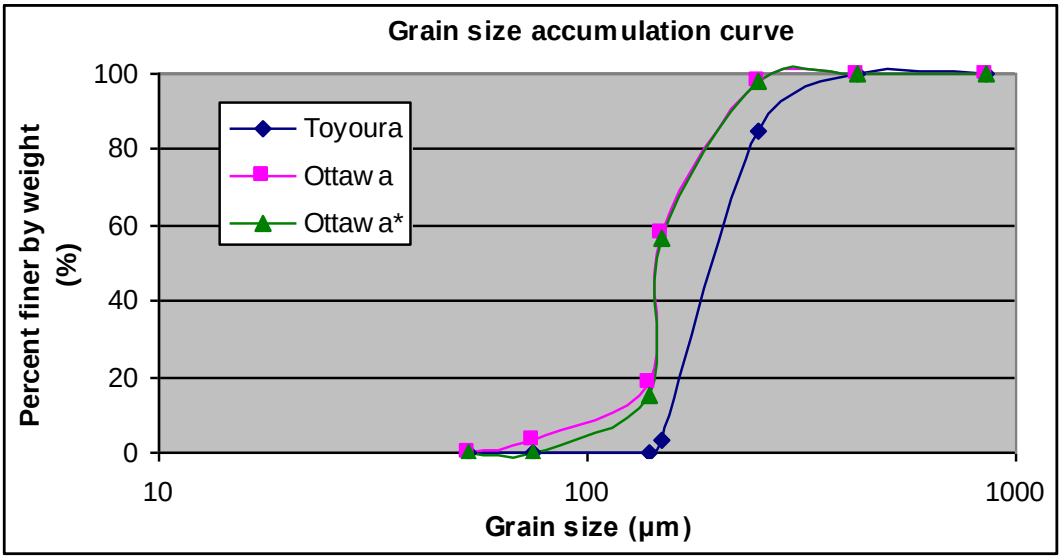

Figure 4.1.1 Sand grain size curves

The water content tests for all sands were conducted on the same day in order to ensure similar ambient conditions. Both Ottawa sand and Ottawa* sand have slightly lower water content than Toyoura sand. This is may be related to their higher silt content. Fine silt particles reduce the void space between particles where moisture collects. The specific gravity of Toyoura and Ottawa sand are given in Table 4.1.1 appear reasonable, since they are silicates whose specific gravity is typically around 2.700 g/cm^3. The small differences in specific gravities may

again be due to fine particles that fill voids between the larger particles in the Ottawa and Ottawa* sands.

Figures 4.1.2 and 4.1.3 are representative SEM images of, respectively, the Ottawa and Toyoura sands at different magnifications. A Hitachi S-4800 field emission SEM operated by the Biological Electron Microscope Facility located at the University of Hawaii at Manoa was employed to document the topographical features of the sand particles. This instrument is also equipped with an Oxford INCA Energy 250 energy-dispersive X-ray spectroscopy system for elemental analysis.

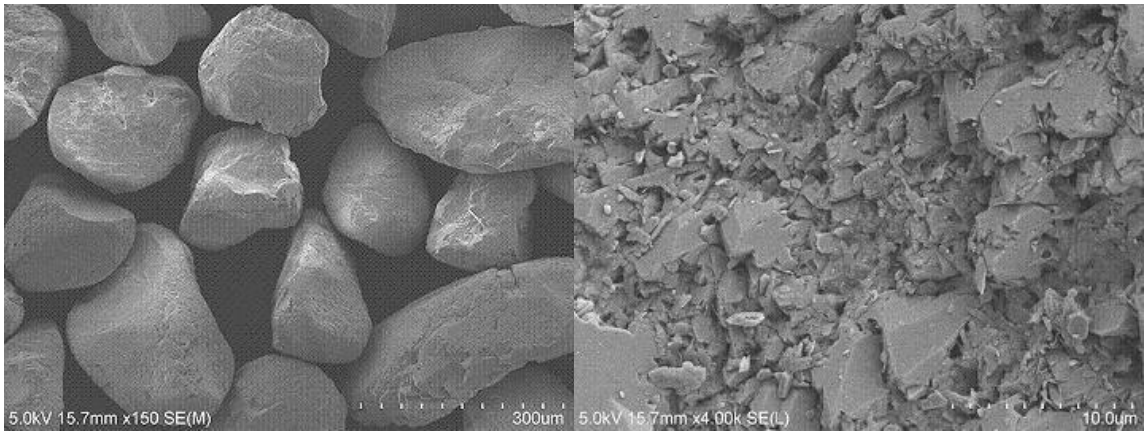

Figure 4.1.2 SEM images of Ottawa sand at two magnifications (see scale)

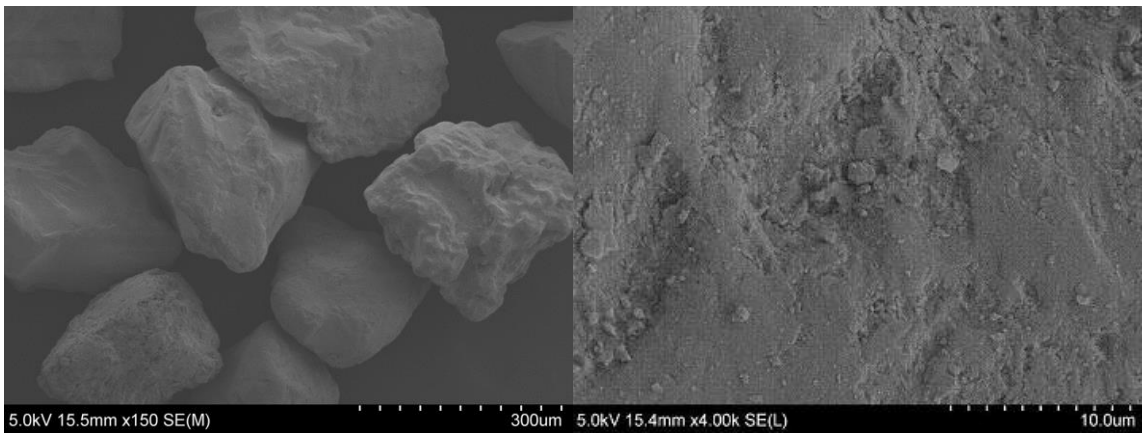

Figure 4.1.3 SEM images of Toyoura sand at two magnifications (see scale).

Both sands have relatively smooth surfaces and are primarily composed of aluminum silicates, which is typical of silicate sand. As seen in the SEM X-ray spectroscopy images (Figures 4.1.4 and 4.1.5), Toyoura sand appears to have more iron than Ottawa sand. In these figures, silicate is colored green, aluminum is blue, and iron is red. These three are the most prominent elements detected in the analysis.

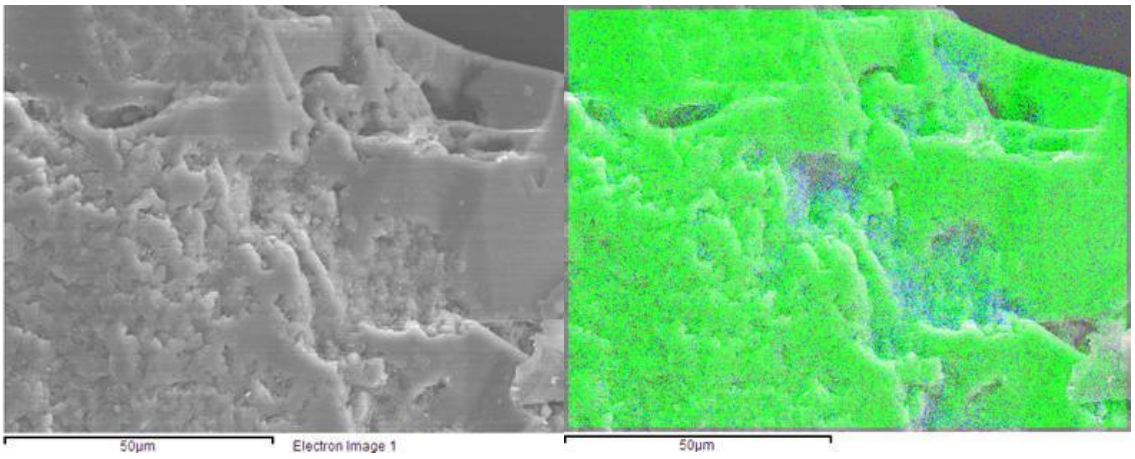

Figure 4.1.4 SEM image of Ottawa sand and overlay view of three elements

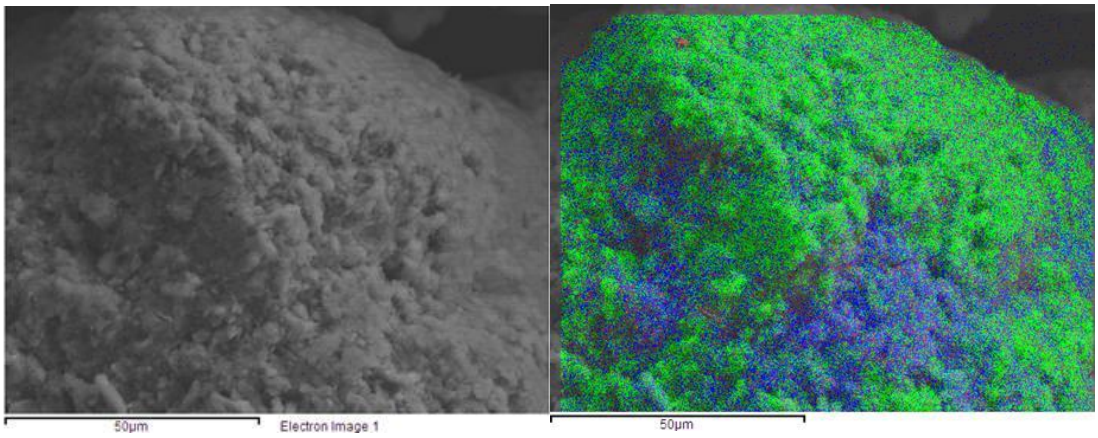

Figure 4.1.5 SEM image of Toyoura sand and overlay view of three elements

In order to determine void fraction and grain porosity, Particle Technology Labs (Downers Grove, IL) performed mercury intrusion porosimetry on replicate aliquots of the sand. The primary results of these analyses are summarized in Table 4.1.2. These data only consider

surface pores < 6 μm. Additional information on sand grain porosity was obtained with a gas adsorption instrument (Micromeritics TriStar 3000). Those data are summarized in Table 4.1.3.

Sample	Total Intrusion Volume [cm^3/g]	Total Pore Area [m^2/g]	Volume Median Pore Diameter [μm]	Bulk Density [g/cm^3]	Apparent Density [g/cm^3]	Percent Porosity n_{int}[%]
Toyoura #1	0.0082	0.38	0.32	1.41	1.43	1.15
Toyoura #2	0.0060	0.11	0.51	1.47	1.49	0.88
Ottawa #1	0.0032	0.25	1.60	1.49	1.49	0.47
Ottawa #2	0.0005	0.003	0.88	1.56	1.56	0.07

Table 4.1.2 Mercury intrusion porosimetry results for Toyoura and Ottawa sands

Sand	Specific surface area (m^2/g)
Ottawa	0.11
Toyoura	0.74

Table 4.1.3 Gas sorption analysis of Toyoura and Ottawa sands

The results of the mercury intrusion porosimetry and gas sorption analyses of the two sands indicate that they have very low grain porosity. The mercury porosimetry data exhibit significant variations between samples of the same sand because of the extremely low measured intrusion volumes that result from the low porosity of the material. The gas sorption data indicate that the specific surface area of the Toyoura sand is larger than that of Ottawa sand; however, both of the sands have very low specific surface areas, indicating that they are essentially non-porous.

4.2. Calorimetry

A series of calorimetry experiments were performed at different pressures between about 450 psig (3.2 MPa) and 1100 psig (7.7 MPa), which correspond to ocean depths between approximately 300 m and 750 m. The primary outcome of these experiments was the measured phase change temperatures for the hydrate at these pressures.

4.2.1 Thermograms and Raman spectra

Figures 4.2.1 and 4.2.2 are representative thermograms from a calorimetry experiment using Ottawa sand. The pressure was set at P = 1000 psi (7.00 MPa) and held constant (±1%) throughout the test. Figure 4.2.1 shows the portion of the process where temperature is slowly reduced over a period of about 5 hours from 23°C (room temperature in the lab) to 1°C. The blue line in the figure is heat flow to or from the sample (mW) as a function of time, the red line is sample temperature (°C), and the purple line is the temperature of the furnace (°C) that is used to supply or remove heat. Heat flow is positive when energy is transferred from the sample cell towards the reference cell, indicating an exothermic process, and negative during an endothermic process. The steep positive peak in the heat flow curve seen in Figure 4.2.1 occurs as a result of hydrate formation. Note that sample temperature is above the ice point.

Figure 4.2.2 shows the portion of the process where sample temperature is very slowly raised from 1°C to 12°C over 16 hours. The large negative (endothermic) heat flow peak that begins at around the 12 hour mark is due to dissociation of the hydrate in the sand. The heat flow peaks in the thermograms at temperatures above the freezing point of water provided substantial evidence of hydrate formation and dissociation.

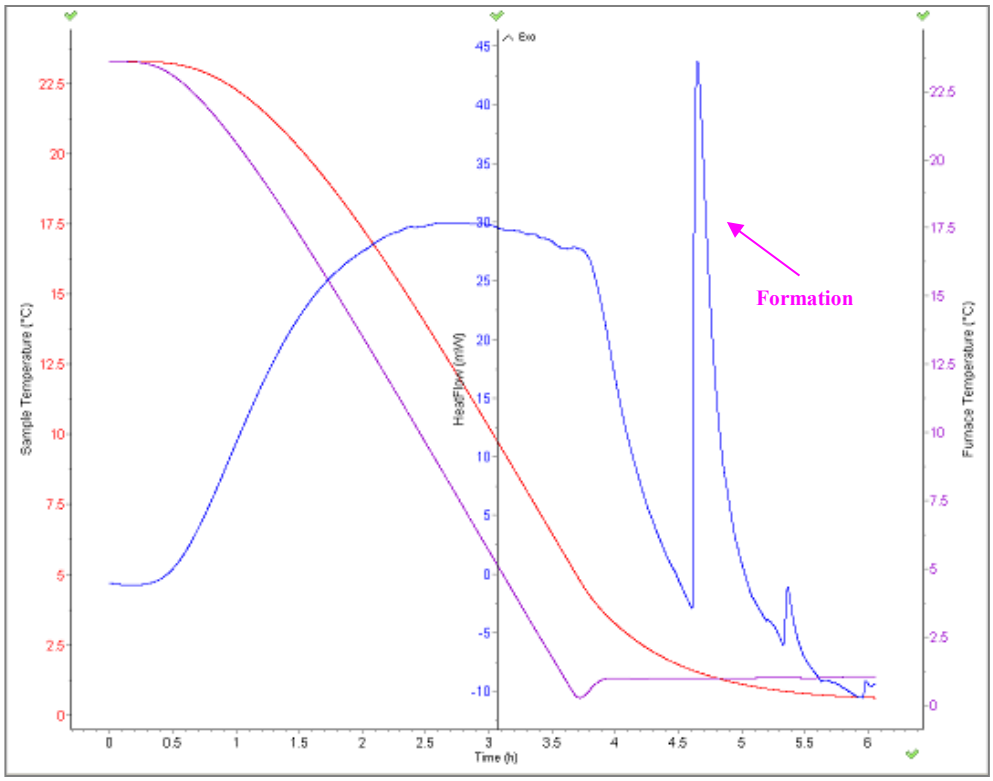

Figure 4.2.1 Calorimetry thermogram of methane hydrate formation in Ottawa sand

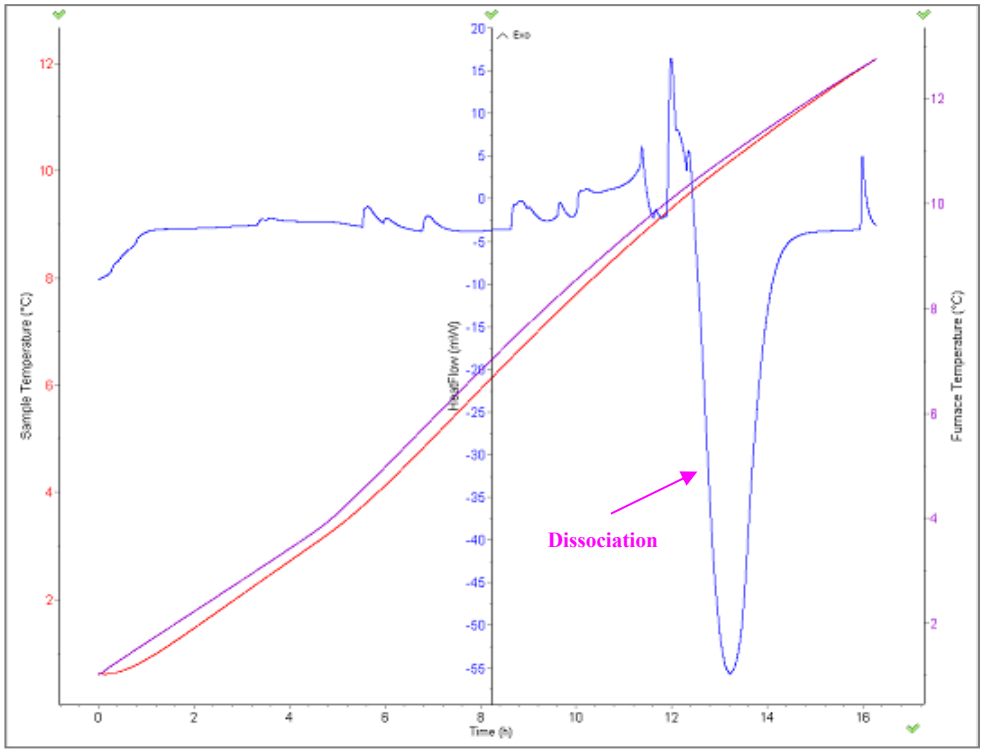

Figure 4.2.2 Calorimetry thermogram of methane hydrate dissociation in Ottawa sand

The presence of hydrate in the sample was confirmed using Raman spectroscopy. An example of the Raman spectra obtained during the experiments with the fiberoptic probe system is shown in Figure 4.2.3. The spectrum exhibits two peaks: the smaller peak to the left (633.90 nm) corresponds to methane hydrate and larger peak (634.31 nm) to methane gas overlying the sample in the calorimeter cell.

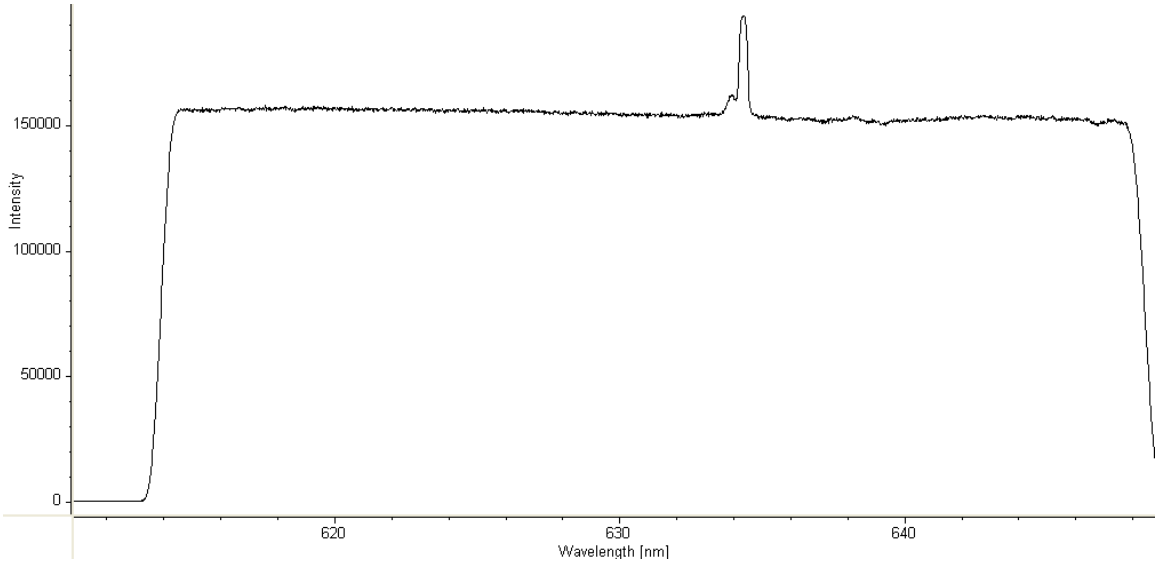

Figure 4.2.3 Raman spectra

4.2.2 Hydrate phase transition temperatures

Hydrate formation is a crystallization process and therefore involves nucleation and growth. Sub-cooling frequently is observed and phase transition data can exhibit significant scatter. Dissociation, on the other hand, is less sensitive to random experimental factors, so the phase transition temperatures were determined from the hydrate decomposition data. The process that was employed to identify melting point temperatures from the calorimetry thermograms is described below by reference to Figure 4.2.4:

i. Extend the baselines of heat flow before and after the hydrate dissociation peak since the temperature ramping rate is constant.

ii. Calculate the average value of the heat flow at the two points of intersection of the curve with these baselines, shown in the figure as green dots, and find the time that corresponds to this average value.

iii. Determine the sample temperature at the time identified in step ii.

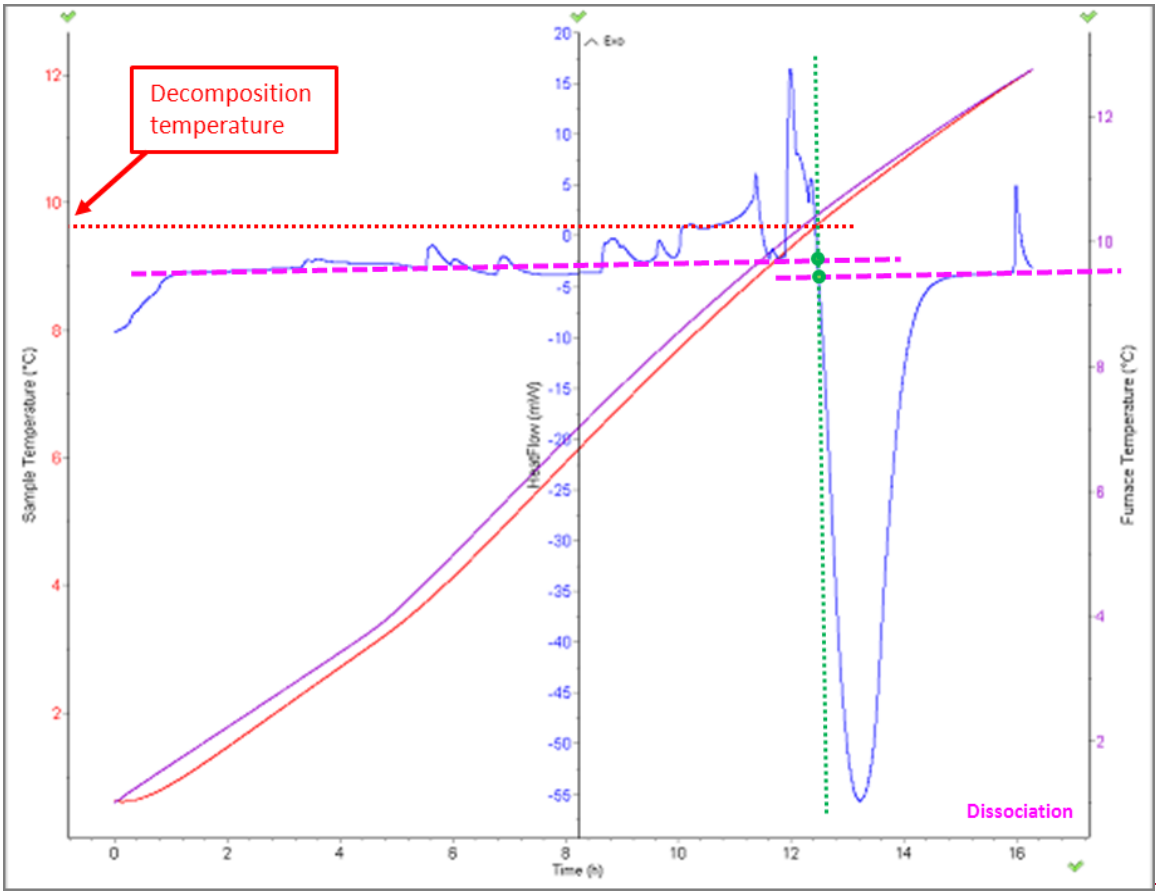

Figure 4.2.4 Determination of the hydrate dissociation temperature

Table 4.2.1 summarizes the calorimeter experiments that were performed in this investigation. Figure 4.2.5 presents the results for the Ottawa and sieved Ottawa* sands. The solid line is the phase boundary for bulk hydrate (no porous media). Although there is significant scatter in the data, measured dissociation temperatures were consistently lower than the values for bulk hydrate at the same pressure. Differences typically fell between 1 and 2°C.

Sand	Mass of sand (g)	Mass of water (g)	Porosity n(%)	Sr (%)	Presssure(psi)	Dissociation temperature (°C)
Ottawa	10.9	2.17	40	80	1001.94	9.5
	10.9	2.17			999.12	9.29
	1.95	0.39			631.47	5.00
	1.95	0.39			628.16	4.90
Ottawa*	10.91	2.17			1012.36	9.75
	10.91	2.17			1011.01	9.68
	10.91	2.17			1010.00	9.40
	5.84	1.16			1042.00	9.08
	2.43	0.48			994.95	9.75
	2.43	0.48			864.83	10.50
Toyoura	10.84	2.17			1006.11	9.6
	10.86	2.17			1013.71	9.25
	2.42	0.48			442.74	0.79
	2.42	0.48			940.25	7.85
	4.48	0.97			1055.53	10.00

Table 4.2.1 Measured dissociation temperatures for different sand and pressures

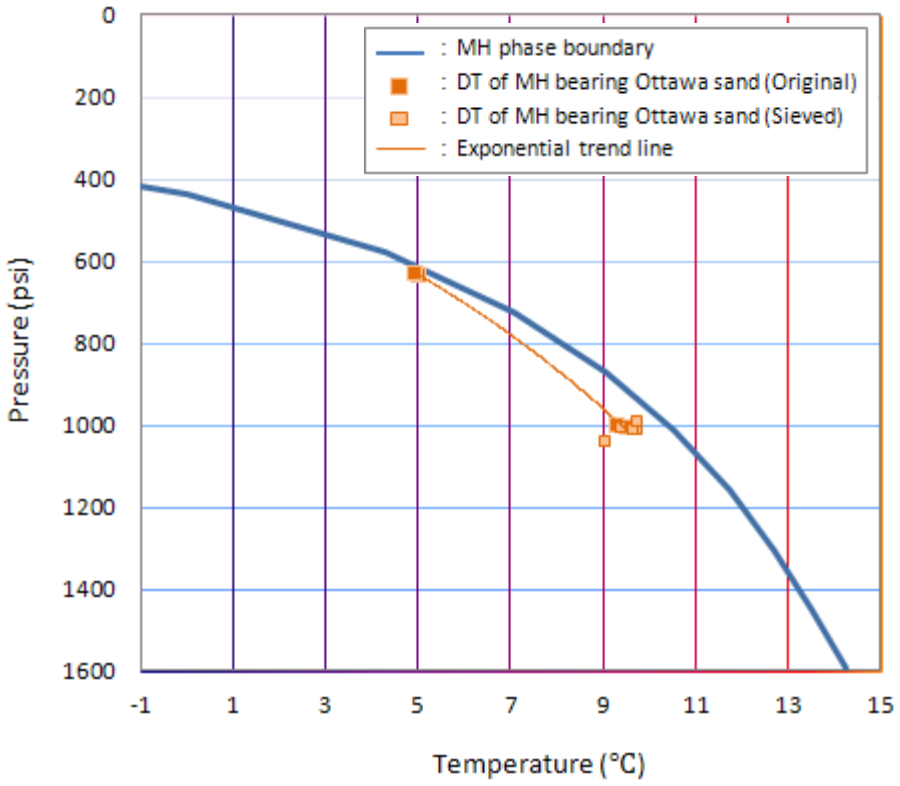

Figure 4.2.5 Measured dissociation temperatures for Ottawa sand

From a different perspective, at a given temperature, the data suggest that methane hydrate in sand dissociates at pressures 15 to 200 psi lower than expected, which is greater than the

uncertainty in the pressure data. Figure 4.2.5 also includes a trend line calculated from all the data points. Finally, the results for the Ottawa and sieved Ottawa* sands do not exhibit any significant differences.

Figure 4.2.6 shows the results for Toyoura sand. With the exception of the single data point at P = 440 psi (3.14 MPa), measured dissociation temperatures were again consistently lower than the values for bulk hydrate at the same pressure. The differences also typically fell between 1 and 2°C (although there is one data point where the difference is significantly larger). The corresponding pressure offsets were > 100 psi. The plotted trend line appears to confirm the shift in the phase boundary. All the experimental data are plotted in Figure 4.2.7.

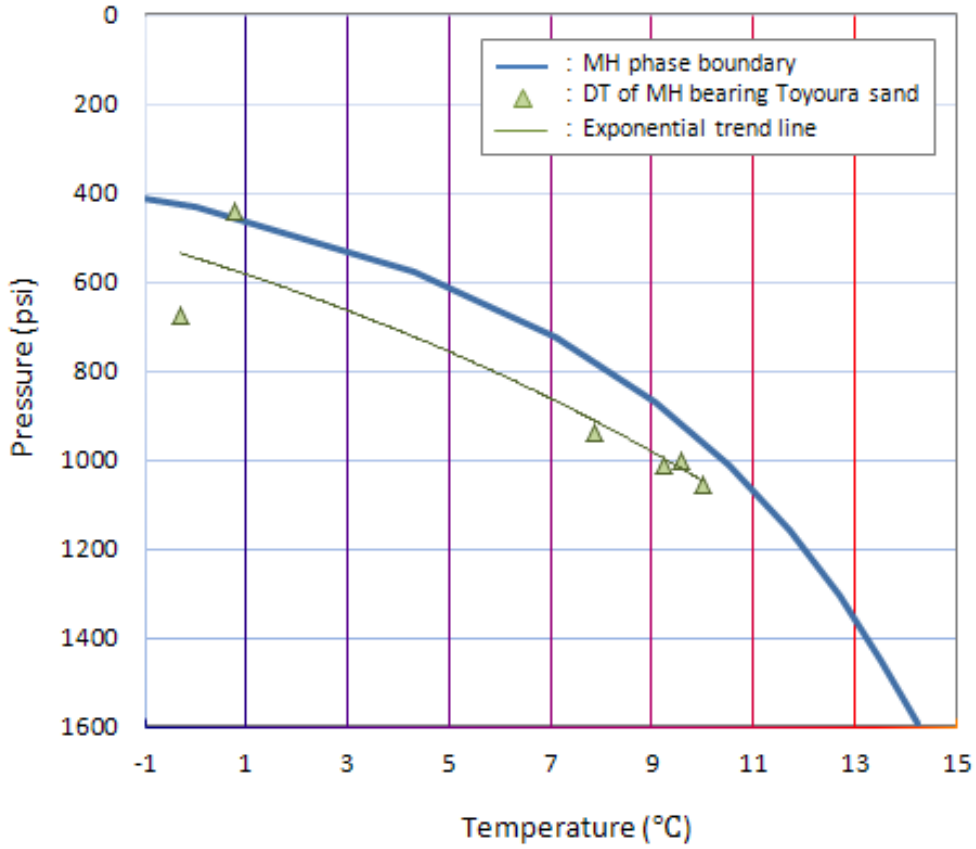

Figure 4.2.6 Measured dissociation temperatures for Toyoura sand

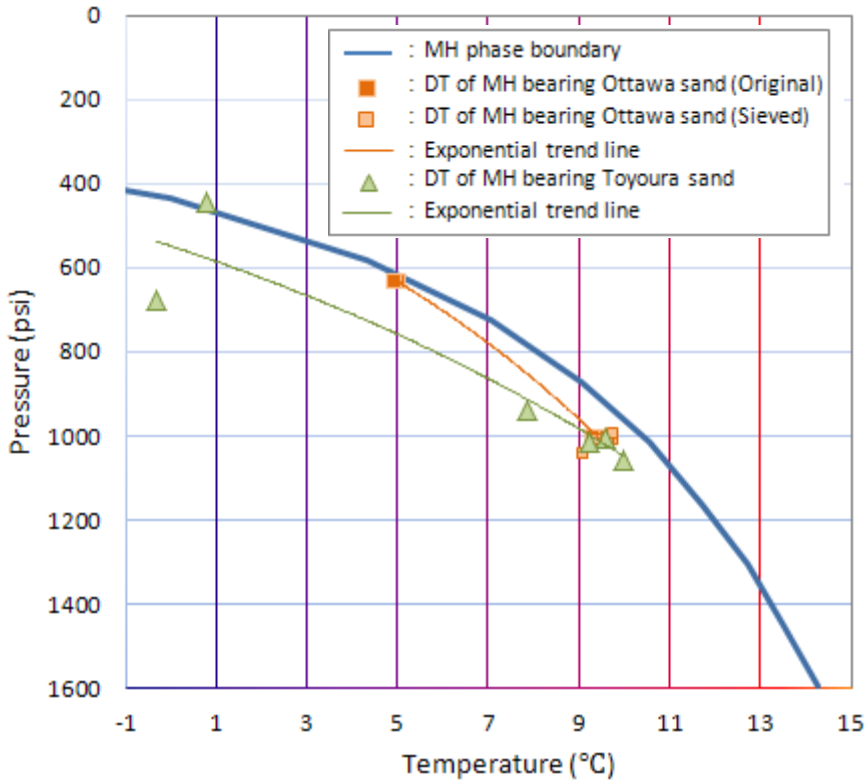

Figure 4.2.7 Measured dissociation temperatures for all experiments

Strategies to recover methane from marine hydrate deposits by thermal stimulation or depressurization, estimates of the volume of the hydrate stability zone in marine sediments to assess reservoir inventories, and assessments of the sensitivity to these reservoirs to changes in deep water temperature typically employ the phase diagram for simple methane-water systems. The results of Uchida *et al*. (2004) and the present investigation suggest this may not be appropriate since methane hydrates appear to form and dissociate at lower temperatures in sand than bulk hydrate.

5. CONCLUSIONS

Calorimetric experiments were performed to test the hypothesis that the pressure-temperature phase boundaries of methane hydrate change when formation and dissociation occur in porous media. Two "standard" sands selected by the national methane hydrate R&D programs in Japan and the U.S. were employed in these experiments. The data suggest that a small shift in the phase boundary of hydrates might occur in porous media. The measured change is of the order of scatter in the experimental data but is consistent. For both sands, and over a range of pressures relevant to deep ocean sediments, the phase boundary for a simple water-methane binary system tends to overpredict hydrate melting temperature.

Lower melting temperatures imply that natural hydrate deposits in seafloor sediment are more vulnerable to purposeful or inadvertent increases in temperature. While this can be advantageous for certain methane recovery strategies, it raises concerns about outgassing and seafloor stability in a warming climate. Additional experiments appear to be warranted to confirm this phenomenon for a broader range of porous media properties and to more definitively quantify the shift in the phase boundary and to understand the underlying mechanism.

Acknowledgments

Funding for this investigation was provided by the Office of Naval Research HEET and APRISES programs.

References

Boswell, R. & Collett, S.T. (2011). Current perspectives on gas hydrate resources. *Energy & Environmental Science*, *4*, 1206-1215.

Handa, Y. P. (1986). Compositions, Enthalpies of Dissociation, and Heat Capacities in the Range 85 to 270 K for Clathrate Hydrates of Methane, Ethane, and Propane, and Enthalpy of Dissociation of Isobutate Hydrate, as Determined by a Heat-Flow Calorimeter. *Journal of Chemical Thermodynamics*, *18*, 915-921.

Hyodo, M., Nakata, Y., Yoshimoto, N., Ebinuma, T. (2005). Basic research on the mechanical behavior of methane hydrate-sediments mixture. *Soils and Foundations, 45 (1)*, 75-85.

Nago, A. & Neito, A. (2011). Natural gas production from methane hydrate deposits using CO_2 clathrate sequestration: State-of-the-Art review and new technical approaches, *Journal of Geological Research, 2011*.

Sloan, E.D. & Koh, C.A. (2007) *Clathrate Hydrates of Natural Gasses* (3rd ed.). Boca Raton, FL: CRC Press.

Takeya, S., Hori, A., Hondoh, T., & Uchida, T., (2000). *Journal of Physics and Chemistry B, 104*, 4164.

Trofimuk, A.A., Cherskii, N.V., Tsarev, V.P., & Nikitin, S.P. (1982). *Geologiva i Geofizika*, *23*, 3.

Uchida, T., S. Takeya, Chuvilin, E.M., Ohmura, R., Nagao, J., Yakushev, V.S., Istomin, V.A., Minagawa, H., Ebinuma, T., & Narita, H. (2004). Decomposition of methane hydrates in sand, sandstone, clays, and glass beads, *J. Geophys. Res.*, *109*, B05206.

Waite, W.F., Winters, W.J., Mason, D.H. (2004). Methane hydrate formation in partially water-saturated Ottawa sand, *American Mineralogist*, *89 (8-9)*, 1202-1207.

Yoneda, J., Hyodo, M., Nakata, Y., Yoshimoto, N., & Orense, R. (2011). Deformation of seabed due to exploitation of methane hydrate reservoir, *Frontiers in Offshore Geotechnics II*, 245-250.